IOP Publishing Journal of Physics: Condensed Matter
J. Phys.: Condens. Matter **26** (2014) 425502 (9pp) doi:10.1088/0953-8984/26/42/425502

Touching points in the energy band structure of bilayer graphene superlattices

C Huy Pham[1,2] **and V Lien Nguyen**[1,3]

[1] Theoretical and Computational Physics Department, Institute of Physics, VAST, 10 Dao Tan, Ba Dinh Distr., Hanoi 10000, Vietnam
[2] SISSA/International School for Advanced Study, Via Bonomea 265, I-34136 Trieste, Italy
[3] Institute for Bio-Medical Physics, 109A Pasteur, 1st Distr., Hochiminh City, Vietnam

E-mail: nvlien@iop.vast.ac.vn

Received 18 June 2014, revised 20 August 2014
Accepted for publication 28 August 2014
Published 2 October 2014

Abstract

The energy band structure of the bilayer graphene superlattices with zero-averaged periodic δ-function potentials are studied within the four-band continuum model. Using the transfer matrix method, the study is mainly focused on examining the touching points between adjacent minibands. For the zero-energy touching points the dispersion relation derived shows a Dirac-like double-cone shape with the group velocity which is periodic in the potential strength P with the period of π and becomes anisotropic at relatively large P. From the finite-energy touching points we have identified those located at zero wave-number. It was shown that for these finite-energy touching points the dispersion is direction-dependent in the sense that it is linear or parabolic in the direction parallel or perpendicular to the superlattice direction, respectively. We have also calculated the density of states and the conductivity which demonstrates a manifestation of the touching points examined.

Keywords: bilayer graphene, superlattice, energy band structure

(Some figures may appear in colour only in the online journal)

1. Introduction

Bilayer graphene shares many properties with monolayer graphene, and has a very high potential for electronic applications such as excellent electric and thermal conductivities at room temperature or the possibility to control the electronic structure externally (see for review [1–4]). However, bilayer graphene (BLG) also exhibits the unique features that make it qualitatively distinct from monolayer graphene (MLG) [3, 4]. For instance, the integer quantum Hall effect in BLG indicates the presence of massive chiral quasi-particles with a parabolic dispersion at low energies (rather than massless quasi-particles with a linear dispersion in MLG). From an application point of view the ability to open a gap in the BLG energy spectrum and to turn it flexibly by an external electric field is exclusively important. It is expected that the BLG-based nano-devices would show the functionalities in a different way to those in the corresponding MLG-based devices. Moreover, with only two layers in the structure the BLG represents the thinnest possible limit of a large class of intercalated materials which have recently been attracting much attention from condensed matter physicists as well as material science researchers [5].

As is well-known, an external periodic potential can essentially modify the energy band structure of materials resulting in unusual transport properties. The energy band structure of MLG under a periodic potential (monolayer graphene superlattice—MLGSL) has been extensively studied in a number of works for the potentials of different natures (electrostatic [6–9] or magnetic [10–14]) and different shapes (Kronig–Penney [6, 9, 11, 14], cosine [7] or square [8]). Interesting discoveries have been reported, such as a strongly anisotropic renormalization of the carrier group velocity and the emergence of extra Dirac points (DPs) in the band structure of electrostatic MLGSLs [6–9] or the emergence of finite-energy DPs in the band structure of magnetic ones [12–14]. Much less work has been devoted to the BLG-superlattices (BLGSLs) [15–17]. Barbier, Vasilopoulos, and Peeters (BVP) introduced the Kronig–Penney model of BLGSLs with δ-function potentials and predicted that either a pair of zero-energy touching points (TPs) is generated or a direct

band gap is opened in the energy spectrum, depending on the strength of the δ-function potentials [15].

In the present paper we study the energy band structure of BLGSLs within the same model of zero-averaged periodic δ-function potentials as that stated by BVP [15] (hereafter referred to as BVP-model for short). Our study however is focused on examining the TPs between adjacent minibands, including the zero-energy TPs claimed before in [15] as well as the finite-energy ones identified first in this work.

The paper is organized as follows. In section 2 we briefly describe the problem being studied within the four-band continuum model and reconsider the zero-energy TPs claimed previously. The dispersion derived in the vicinity of these points shows a Dirac-like double-cone shape with the group velocity which is periodic in the potential strength P with a period of π and becomes strongly anisotropic at relatively large P. In section 3 we show that for any finite potential strength there are always finite-energy TPs at zero wave number, ($k = 0$), regardless of whether there are zero-energy TPs or whether there is a band gap. Impressively, the dispersion associated to these TPs is direction-dependent in the sense that in one direction the dispersion is linear whereas in other directions it is parabolic. Section 4 presents the density of states and the conductivity that demonstrates possible manifestations of the touching points examined. The paper closes with a brief summary in section 5.

2. Four band Hamiltonian and zero-energy Dirac points

We consider BLGSLs arising from an infinitely flat Bernal-stacked BLG in a periodic one-dimensional potential $V(x, y) \equiv V(x)$. Within the continuum nearest-neighbour tight-binding model the four-band Hamiltonian describing low-energy excitations near one Dirac point (say, K) for these BLGSLs has the form:

$$H = \begin{pmatrix} 0 & v_F\hat{\pi} & t_\perp & 0 \\ v_F\hat{\pi}^+ & 0 & 0 & 0 \\ t_\perp & 0 & 0 & v_F\hat{\pi}^+ \\ 0 & 0 & v_F\hat{\pi} & 0 \end{pmatrix} + V(x)\mathcal{I}, \qquad (1)$$

where $\hat{\pi} = p_x + \mathrm{i}p_y$, $p = (p_x, p_y)$ is the in-plane momentum, $v_F = \sqrt{3}ta/(2\hbar) \approx 10^6\,\mathrm{m\,s^{-1}}$ is the Fermi velocity, $t \approx 3\,\mathrm{eV}$ is the intralayer nearest-neighbour hopping energy, $a = 2.46\,\text{Å}$ is the lattice constant of graphene, $t_\perp \approx 0.39\,\mathrm{eV}$ is the interlayer nearest-neighbour hopping energy, and $\mathcal{I}$ is the identity matrix. Other interlayer hopping parameters are neglected here since they are much smaller than $t_\perp$ and may be effectively suppressed by disorder [2, 4, 18]. Also, this Hamiltonian is limited to the case of symmetric on-site energies.

Without the potential $V(x)$, i.e. for pristine BLG, the Hamiltonian of equation (1) yields the hyperbolic band dispersion which interpolates between a linear dispersion at large momentum and a quadratic one at small momentum [4]. Such a hyperbolic BLG band dispersion was experimentally recognized in different measurements, cyclotron resonance of electrons and holes [19] or electric compressibility [20]. Interestingly, the hyperbolic shape of BLG band dispersion still seems to survive (with renormalized parameters) even if the electron–electron interaction is taken into account [18, 21]. We are interested here in the effects induced by a periodic potential on the BLG non-interacting band structure.

The potential $V(x)$ under study is the zero-averaged periodic δ-function potential with strength P and period L defined as (see figure 1(a)):

$$V(x) = P\left\{\sum_n \delta(x - nL) - \sum_n \delta[x - (n + 1/2)L]\right\}. \qquad (2)$$

In fact, this potential model is exactly the one introduced by BVP (BVP-model) [15]. These authors claimed that in studying the energy band structure of (at least) BLGSLs with the δ-function potentials, the two-band approximation (see for example [4]) is not accurate enough and the four-band Hamiltonian of equation (1) should be applied.

Due to a periodicity of the potential $V(x)$ (equation (2)) the time-independent Schrödinger equation $H\Psi = E\Psi$ for the Hamiltonian H of equation (1) could be most conveniently solved using the transfer matrix approach [15, 22]. This approach reduces the energy spectrum problem to solving the equation (see appendix A):

$$\det\,[\,T - \mathrm{e}^{\mathrm{i}k_x L}R_I^{-1}(L)\,] = 0, \qquad (3)$$

where k_x is the Bloch wave vector, L is the period of the potential $V(x)$ (equation (2)), and T and R_I are matrices, depending on the Hamiltonian of interest (see appendix A).

In the case of MLGSLs, when the Hamiltonian H and, therefore, T and R_I are 2×2 matrices, equation (3) can be analytically solved to immediately give a general expression for the dispersion relation $E(\vec{k})$ [9, 14]. For BLGSLs in the four-band model of equation (1), equation (3) with (4×4)-matrices T and R_I becomes too complicated. In general it cannot be solved analytically and, therefore, the dispersion relation cannot be derived explicitly. We have numerically solved equation (3) and show in figures 1(b)–(d) the lowest conduction and the highest valence minibands obtained for some values of the potential parameters P and L. Hereafter, we introduce the dimensionless variables: $E \to E/t_\perp$, $V \to V/t_\perp$, $x(L) \to x(L)/(\hbar v_F/t_\perp)$, and $k_{x(y)} \to k_{x(y)}/(t_\perp/\hbar v_F)$ with $t_\perp$ and v_F given above.

The most impressive feature observed in figure 1 is that, instead of the original zero-energy DP of the pristine BLGs at $\vec{k} = 0$ a pair of new TPs appeared in the ($k_y = 0$)-direction (figures 1(b) and (c)) or a direct band gap appeared (figure 1(d)), depending on the values of P and L. Actually, such a picture of the zero-energy TPs or the band gap has been reported before by BVP [15] and it is included here for additional discussions. Before going over to detailed considerations we would like to note that due to the symmetry of the periodic potential $V(x)$ of equation (2) (with a zero spatial average) the energy spectrum of the BLGSLs under study should be symmetric with respect to the sign of energy. This results in a double-cone shape of band dispersions in the vicinity of all the existing zero-energy TPs.

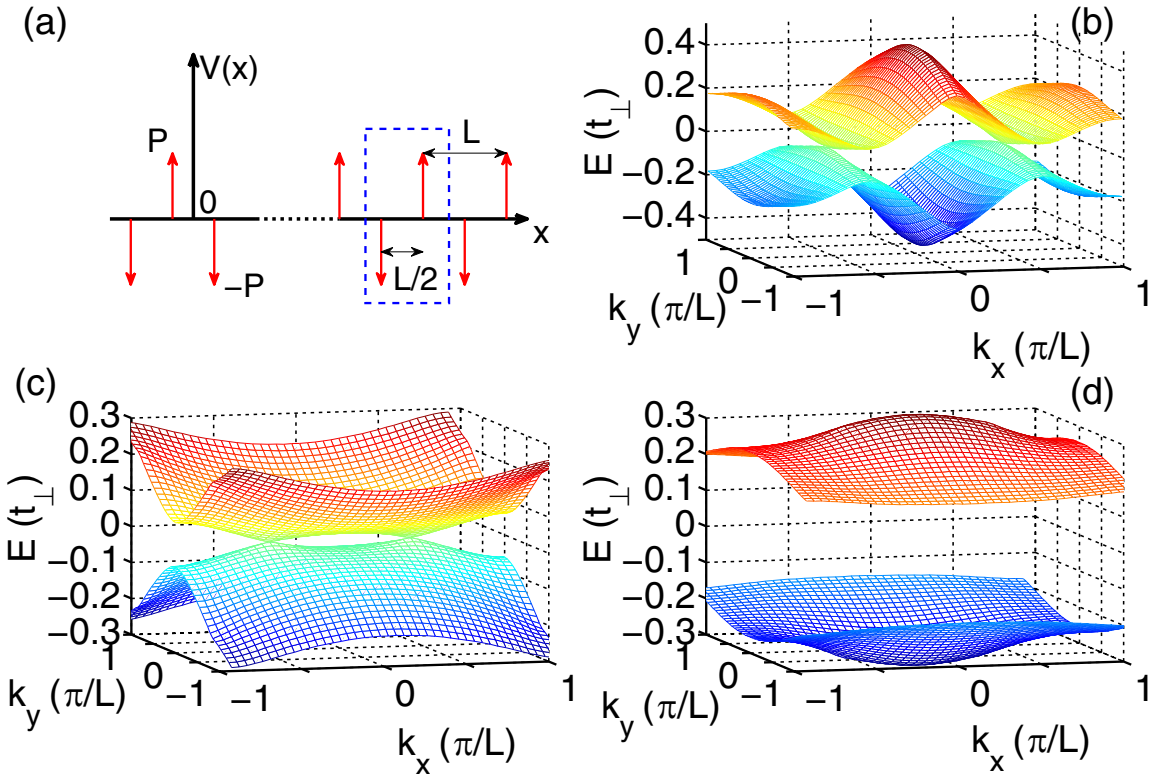

Figure 1. (*a*) Schematics of a zero-averaged periodic δ-function potential $V(x)$ with strength P and period L (the dashed-line box describes the unit cell in the T-matrix calculation); (*b*)–(*d*) are the energy spectra of the lowest conduction and highest valence minibands for BLGSLs with $[L = 3,\ P = 1.5]$, $[L = 8,\ P = 0.1\pi]$, and $[L = 8,\ P = 0.4\pi]$, respectively. For $L = 8 > L_C$ either a pair of zero-energy DPs is generated (*c*) or a direct band gap opens up (*d*), depending on P. For $L < L_C$ a pair of zero-energy DPs always existed, regardless of P.

Next, in order to understand the new zero-energy TPs generated in the $(k_y = 0)$-direction (figures 1(*b*) and (*c*)) or the direct band gap opened at some values of L and P (figure 1(*d*)), following BVP [15] we consider the energy spectrum along the $(k_y = 0)$-direction. In this case, in the wave function $\Psi = (\psi_{A_1}, \psi_{B_1}, \psi_{B_2}, \psi_{A_2})^T$ the two components relating to the first layer (ψ_{A_1}, ψ_{B_1}) and those to the second layer (ψ_{B_2}, ψ_{A_2}) become decoupled and, therefore, the energy spectrum can be obtained in the form of the transcendental equations[4]:

$$\cos(k_x L) = \cos^2(k_n L/2) - \sin^2(k_n L/2) D_n, \quad n = 1 \text{ and } 2, \tag{4}$$

where $D_n = \cos^2 P + [(E^4 + k_n^4)/(2E^2 k_n^2)] \sin^2 P$ and $k_n = \sqrt{E^2 - (-1)^n E}$. (In these equations all variables are dimensionless as defined above).

Due to the symmetry of the energy spectrum with respect to the zero-energy plane it is possible to identify the zero-energy TPs by taking the limit $E \to 0$ in the dispersion relation. Indeed, in this limit any of the equations (4) give to the possible zero-energy TPs the k_x-coordinate that depends on the periodic potential parameters as

$$k_x = \pm k_x^{(0)}(P, L) = \pm \arccos[1 - (L^2/8) \sin^2 P]/L. \tag{5}$$

[4] Notice that equation (4) in this work and the corresponding equation (31) in [15] are unidentified, although all results deduced from them, including equations (5) and (6), are respectively coincided. Surprisingly, we failed to reproduce these results starting from equation (31) in [15].

This equation yields the real values for $k_x^{(0)}$ and, therefore, identifies the position of zero-energy TPs only if the strength P and the period L of the potential $V(x)$ obey the following condition:

$$|1 - (L^2/8) \sin^2 P| \leqslant 1 \text{ or } L^2 \sin^2 P \leqslant 16. \tag{6}$$

Whenever this condition is fulfilled, instead of a single zero-energy DP at $\vec{k} = 0$ (i.e. the K-point) in the energy spectrum of the pristine BLG, the periodic potential $V(x)$ induces a pair of new zero-energy TPs located symmetrically at $k_x = \pm k_x^{(0)}$ along the $(k_y = 0)$-direction. A violation of the condition (6) means there are no zero-energy TPs at all or, in other words, a direct band gap should be opened instead.

Note that the condition of equation (6) is always fulfilled for $L < L_C = 4$. So, for any BLGSL with such a small potential period, $L < L_C (\approx 6.75\,\text{nm}$ given $t_\perp \approx 0.39\,\text{eV})$, there are always in the energy spectrum a pair of zero-energy TPs located at $(k_x = \pm k_x^{(0)}, k_y = 0)$, regardless of the potential strength P. This is the case shown in figure 1(*b*) for the BLGSL with $L = 3$ and $P = 1.5$. Changing P in this figure does not remove the pair of zero-energy TPs, but only shifts their k_x-coordinates.

On the contrary, for any BLGSL of $L > L_C$, with increasing P, the two zero-energy TPs, generated initially near the $(\vec{k} = 0)$-point, move away from this point in opposite directions along the $(k_y = 0)$-direction (figure 1(*c*)). At the potential strength $P = P_C$ defined by the upper limit in the condition of equation (6), $\sin^2 P_C = 16/L^2$, these TPs reach

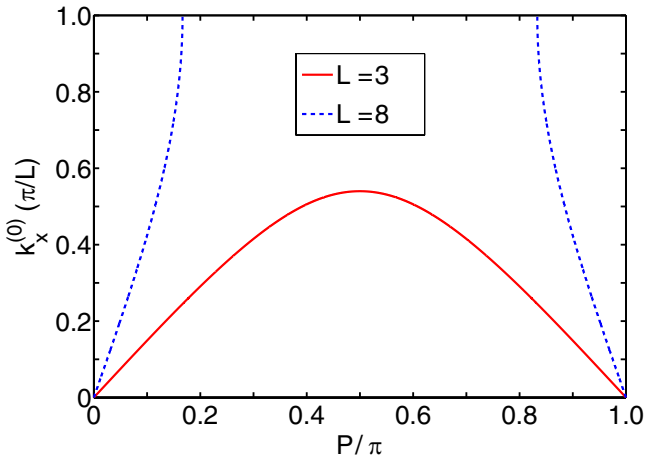

Figure 2. $k_x^{(0)}$ of equation (5) (in unit of π/L) is plotted as a function of P/π in two cases: $L = 3$ (red solid line) and $L = 8$ (blue dashed line). $k_x^{(0)}$ is periodic in P with the period of π.

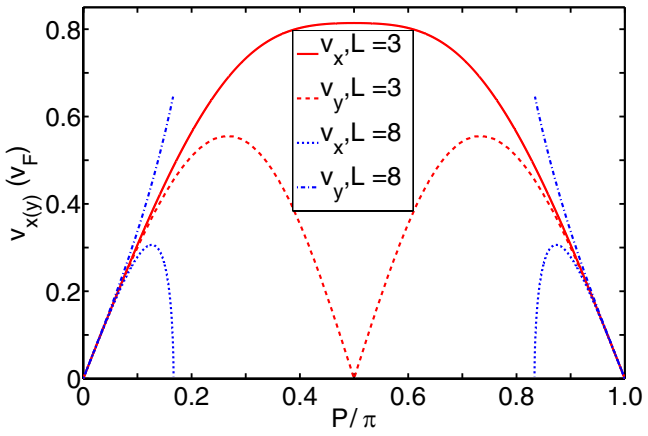

Figure 3. For zero-energy DPs: velocities v_x of equation (8) and v_y (numerically calculated) (in units of v_F) as the functions of the P/π for BLGSLs with: $L = 3$ (v_x—red solid line, v_y—red dashed line) and $L = 8$ (v_x—blue dotted line, v_y—blue dash–dotted line). Velocities are periodic in P with the period of π.

the edge of the Brillouin zone at $k_x = \pm\pi/L$. A further increase in P opens a direct band gap (figure 1(*d*)).

In order to see the whole evolution picture of the zero-energy TP positions and/or the band gap as P varies, we comment on the two properties of the $k_x^{(0)}(P)$-function defined in equation (5): (*i*) $k_x^{(0)}(P) = k_x^{(0)}(P \pm n\pi)$ with n integer number and (*ii*) $k_x^{(0)}(P) = k_x^{(0)}(\pi - P)$. The former property simply means that the whole $k_x^{(0)}(P)$-picture is periodic in P with the period of π and therefore it is enough to examine the $k_x^{(0)}(P)$-dependence in one period, $P \in [0, \pi]$. The latter shows the symmetry of the $k_x^{(0)}(P)$-picture in one period with respect to the middle point $P = \pi/2$. These symmetries can clearly be seen in figure 2 where $k_x^{(0)}$ of equation (5) is plotted versus P in a period for $L = 3$ (red solid line) and $L = 8$ (blue dashed line). In the case of $L = 3 < L_C$ the solid line shows a continuous and regular oscillation of $k_x^{(0)}$ between the minimum of zero at $P = n\pi$ and the maximum of $\pi/2L$ at $P = \pi/2$. In the case of $L = 8 > L_C$ the dashed line shows the P-dependence of $k_x^{(0)}$ in the two symmetrical regions, $0 < P < P_C$ ($\approx 0.167\pi$ in figure 2) and $\pi - P_C < P < \pi$, when the zero-energy TPs are surviving. For the potential strengths in the middle region, $P_C < P < \pi - P_C$, a direct band gap opens up.

Note that the picture similar to the dashed line in figure 2 was previously presented together with the band gap size in figure 12 in [15], where the only case of $L = 10\,\text{nm} > L_C$ is discussed. Note also that the relations of equations (5) and (6) as well as the results presented in figures 1 and 2 are exactly the same as those reported in [15], although, as mentioned above[5], the equations (3) and the corresponding equations (31) in the reference cited are unidentified as yet.

Furthermore, to search for a more accurate understanding of the new zero-energy TPs recognized, we expand equation (3) to the lowest order in E and k_x in the vicinity of these TPs to reveal the linear dispersion relation

$$E^2 = (k_x - k_x^{(0)})^2 v_x^2 + k_y^2 v_y^2, \tag{7}$$

[5] See footnote 4.

where the velocity v_x can be deduced by expanding equation (4):

$$v_x = \frac{\sin P\sqrt{16 - L^2 \sin^2 P}}{4 - (L^2/12)\sin^2 P}, \tag{8}$$

whereas v_y could be numerically calculated. Due to the Dirac-like form of the dispersion relation of equation (7) the zero-energy TPs could really be referred to as the DPs.

Figure 3 presents v_x and v_y in one period of P for the BLGSLs with periods of $L = 3 < L_C$ (v_x—red solid and v_y—red dashed line) and $L = 8 > L_C$ (v_x—blue dotted and v_y—blue dash-dotted line). Noticing that like $k_x^{(0)}$ these velocities are periodic in P with the period of π and, additionally, in one period they are symmetric with respect to the middle point $P = \pi/2$, it is sufficient to analyse the picture in a half of the period. Clearly, in both of the cases under consideration the two curves $v_x(P)$ and $v_y(P)$ are practically coincided at small P, indicating an isotropy of the Dirac cones in this region of P-values. However, with increasing P, two velocities become largely separated, showing a strong anisotropy of the Dirac cones in cases of large potential strength P. Thus, figure 3 demonstrates an interesting feature of the new zero-energy DPs: given a potential period L the dispersion cone is practically isotropic at small potential strength P and becomes strongly anisotropic at large P (Actually, the value P_s below which the dispersion could be considered isotropic depends slightly on L: in figure 3 $P_s \approx 0.08\pi$ or 0.06π for $L = 3$ or $L = 8$, respectively.).

Figure 3 also demonstrates that for small P [$P \leqslant 0.06\pi$] the velocities are not only isotropic, but also almost independent of L. At larger P, there is a strong difference in the velocity behaviour between the BLGSLs with $L > L_C$ and those with $L < L_C$. For the former BLGSLs, v_y increases, while v_x goes back to zero with the opening of the band gap. For the latter, when the gap is totally absent, v_x reaches the maximum, while v_y goes to zero at $P = \pi/2$, implying that the dispersion turns out to be one-dimensional at this value

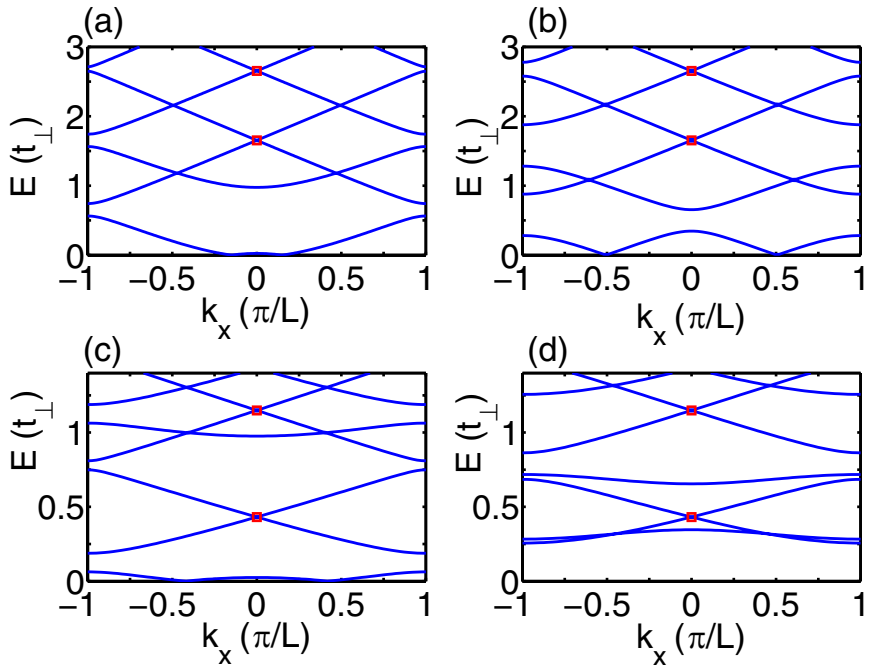

Figure 4. Cuts of the band structure along the $(k_y = 0)$-plane for BLGSLs with different L and P: (a)–(d) for $[L, P] = [3, 0.1\pi]$, $[3, 0.4\pi]$, $[8, 0.1\pi]$, and $[8, 0.4\pi]$, respectively. The lowest finite-energy touching points of equation (9) are marked by the red squares (the spectrum is symmetric with respect to the sign of the energy and only the positive energies are shown). The energy E and the wave number k_x are in units of $t_\perp$ and π/L, respectively. Note, apart from the finite-energy touching points marked, there are also those at $k_x \neq 0$.

of P. Such a difference in the velocity behaviour should find itself reflected in the transport properties.

Actually, the fact that a pair of new zero-energy DPs appeared at small potential strengths or a direct band gap opened at higher ones was also reported in the energy spectra of BLGSLs with different periodic potential shapes, rectangular [16] or sine [17]. Perhaps it could be seen as the common feature in energy band structures of all BLGSLs with zero-averaged periodic potentials. The detailed behaviour of the zero-energy DPs and/or the band gap is however dependent on the potential shape. In particular, for the sine potential within the two-band continuum model, Tan *et al* demonstrated an emergence of new zero-energy DPs even along the $(k_x = 0)$-direction at higher values of the potential strength (see figure 3 in [17]). It is worth mentioning that such zero-energy DPs at $k_x = 0$ should not exist in the band structure of the BLGSLs with periodic δ-function potentials we are interested in[6].

3. Finite-energy touching points

In figure 4 we plot the cuts of the band structure along the $(k_y = 0)$-plane, calculated numerically from equation (3) for various values of the potential strength P (0.1π in (a) and (c); 0.4π in (b) and (d)) or the potential period L (3 in (a) and (b); 8 in (c) and (d)). This figure is focused on showing several minibands next to the lowest one. (Due to the symmetry of energy spectra with respect to the zero-energy plane only the positive energies are shown). Interestingly, in all boxes with different P and/or L in figure 4 apart from the zero-energy DPs described in the previous section, the degeneracy points appeared at finite energies, the TPs of adjacent minibands. Such TPs do exist even when there is no zero-energy DP at all in the energy spectrum (see figure 4(d) for $L = 8$ and $P = 0.4\pi$).

It seems that among the finite-energy TPs observed in figure 4 there is a class of TPs which could be exactly identified. Indeed, equation (4) always has solutions with energies corresponding to the equality $\sin(k_n L/2) = 0$. These energies are then determined as

$$E_\nu^{(i,j)} = \frac{1}{2}\left[(-1)^i + (-1)^j\sqrt{1 + 16\nu^2\pi^2/L^2}\right], \quad i, j = 1, 2; \quad \nu = 1, 2, 3, \cdots \tag{9}$$

which are just the energy positions of all possible finite-energy TPs located at zero wave-number (some of these points are marked by the red square in figure 4). Note that the energies $E_\nu^{(i,j)}$ (9) only depend on L, so in the energy spectra of all BLGSLs with a given L the energy-positions of the TPs, associated with the same indexes ν, i and j, are exactly coincident. (Compare the marked TPs in the two boxes in the same line in figure 4).

Generally, to examine the dispersion behaviour at a TP we should expand equation (3) in the vicinity of this point. As a demonstration, we consider the lowest from all the TPs discussed, the point $E_1^{(1,2)} = [-1 + \sqrt{1 + 16\pi^2/L^2}]/2$ (the lowest red-square in all the boxes in figure 4). Keeping $k_y = 0$, we expand equation (4) in the vicinity of the point $(E = E_1^{(1,2)}, k_x = 0)$ that gives

$$E - E_1^{(1,2)} = \pm k_x v_x, \tag{10}$$

[6] We have examined this problem for BLGSLs with rectangular potentials studied in [16] and we learned that for this potential the zero-energy DPs exist in the $(k_x = 0)$-line at large potential magnitudes, similar to those observed for the sine potential in [17].

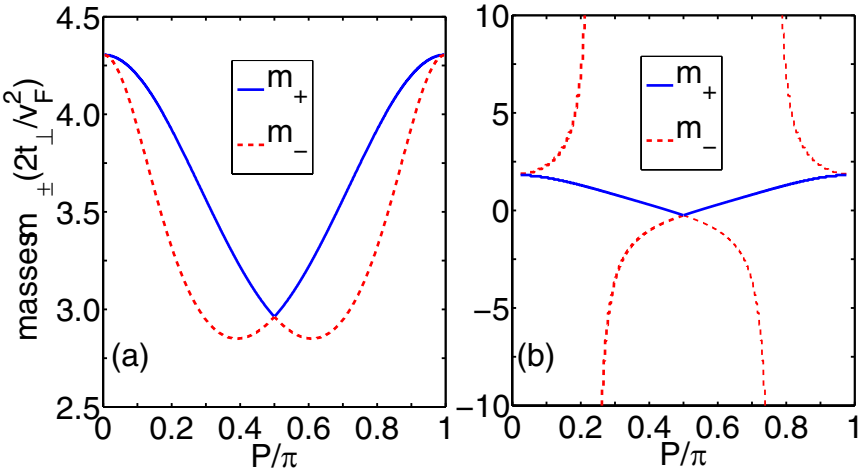

Figure 5. The masses $m_\pm$ in equation (12) (in units of $(2t_\perp/v_F^2)$) for the touching point at $E = E_1^{(1,2)}$ periodically depend on P with the period of π in two cases: $L = 3$ (a) and $L = 8$ (b). In both cases (boxes): a blue solid line describes m_+, while a red dashed line describes m_-.

where

$$v_x = \left[(L^2/16\pi^2 + 1)(L^2 \sin^2 P/16\pi^2 + 1)\right]^{1/2}. \qquad (11)$$

On the other hand, keeping $k_x = 0$ we can expand equation (3) in the vicinity of the point $(E = E_1^{(1,2)}, k_y = 0)$. This can be done only numerically, writing equation (3) in the form of $f(E, k_y) = 0$ (see for detail [9, 14]). It seems that the function f has the zero first derivative, $\partial f/\partial k_y = 0$, so we can readily write

$$E - E_1^{(1,2)} = k_y^2/2m_\pm\,, \qquad (12)$$

with $m_\pm$ being the masses of the parabolic dispersions (the signs $\pm$ at m are corresponding to $\pm$ in equation (10)).

Thus, around the TP located at $E = E_1^{(1,2)}$ the dispersion seems to be direction-dependent in the sense that it is (Dirac-like) linear in the k_x-direction (equation (10)), but parabolic in the k_y-direction (equation (12)). While the velocity v_x in equation (10) is well defined (equation (11)), the manner in which the two minibands touch each other at $E_1^{(1,2)}$ is still associated with the masses $m_\pm$ in equation (12). Unfortunately, we are unable to analytically estimate $m_\pm$, so we present in figure 5 the numerical results of these masses plotted as a function of P in two cases: (a) $L = 3 < L_C$ and (b) $L = 8 > L_C$. In both cases, figure 5 demonstrates that (i) the masses $m_\pm$ exhibit the same symmetric properties with respect to P as $k_x^{(0)}(P)$ in figure 2 or $v_{x(y)}(P)$ in figure 3 and (ii) the two masses are equal, $m_+ = m_-$, at a single point $P = \pi/2$. In the case of $L = 3$ (figure 5(a)), when the band gap never appears, the two masses are both positive, but generally different in value. In the case of $L = 8 > L_C$ (figure 5(b)), when the band gap appears at $P_C < P < \pi - P_C$, the two masses $m_\pm$ may be different in both value and sign, depending on P.

Actually, the dispersion relations of equations (10) and (12) are qualitatively applied for all the TPs located at zero wave-number and at energies defined in equation (9) (but certainly with different v_x and $m_\pm$). Consequently, all the properties identified above for the lowest TP at $E_1^{(1,2)}$ should be qualitatively applied for the whole class of finite-energy TPs of interest.

In fact, the TPs with direction-dependent cones have been reported for various graphynes [23, 24]. In particular, for the TP at the M-point in the spectrum of γ-graphyne the cone was shown to be direction-dependent in a way similar to equations (10) and (12): the dispersion is linear in the $(M-\Gamma)$-direction, but parabolic in the $(M - K)$-one (figure 2 in [24]).

4. Density of states and conductivity

With the energy band structures determined we calculated the density of states (DOS) and furthermore the low temperature conductivity. The calculations were performed in the same way as those suggested for MLGSLs in [11].

Figure 6 presents the DOS of the BLGSLs in two typical cases: (a) $L = 3 < L_C$, when a pair of the zero-energy DPs always existed, regardless of P and (b) $L = 8 > L_C$, when there is either a pair of zero-energy DPs or a direct band gap, depending on P. In each box the three DOS-curves are shown for comparison: the dashed line for the pristine BLG $(P = 0)$; the red solid line for $P = 0.1\pi$; and the blue dash-dotted line for $P = 0.4\pi$. The arrows indicate the energy-positions $E = E_1^{(1,2)}$ of the lowest finite-energy TP defined in equation (9) (this energy does not depend on P, so it is the same for both the red solid and the blue dash-dotted curves in each box.). Notice that the DOSs are symmetric with respect to the zero-energy.

In general, the DOSs of BLGSLs in figure 6 display a fluctuating behaviour, compared to the DOS of the pristine BLG (dashed curves). Notice that a similar fluctuation was reported by BVP in the DOS of MLGSLs [8]. The central minimum (at $E = 0$) is related to the zero-energy DPs or the band gap (the blue dash-dotted curve for $P = 0.4\,\pi$ in (b)). The local dips at finite energies are corresponding to the finite-energy TPs at $k_y = 0$ (either those at $k_x = 0$ identified above or those at $k_x \neq 0$ as can be seen in figure 4), whereas the peaks are located at the bending points between these TPs. In

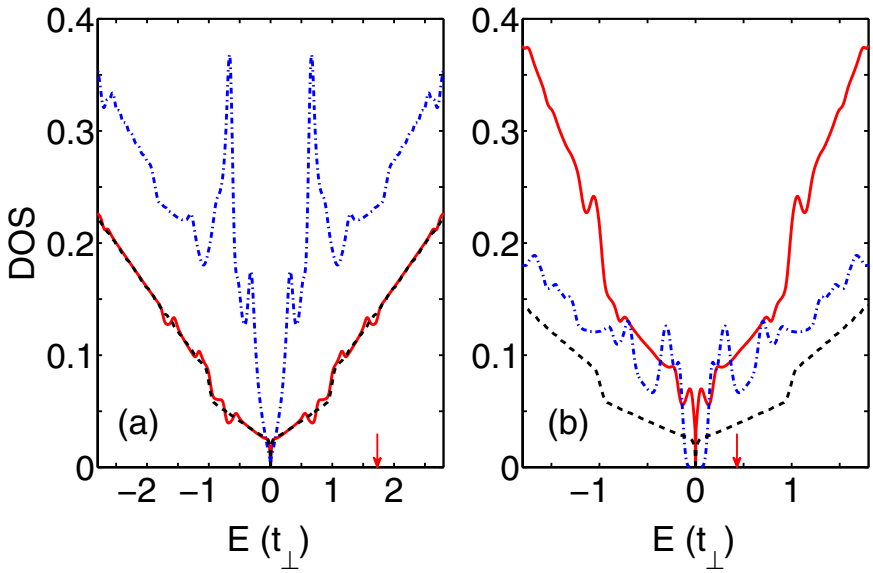

Figure 6. Densities of states are shown for the BLGSLs with different L and P: (a) $L = 3$ and (b) $L = 8$; red solid lines—$P = 0.1\pi$ and blue dash–dotted lines—$P = 0.4\pi$. In both boxes the DOS for the pristine BLG (without periodic potential) is also shown for comparison (dashed line). Arrows indicate the energy $E_1^{(1,2)}$ of the lowest finite-energy touching point of interest.

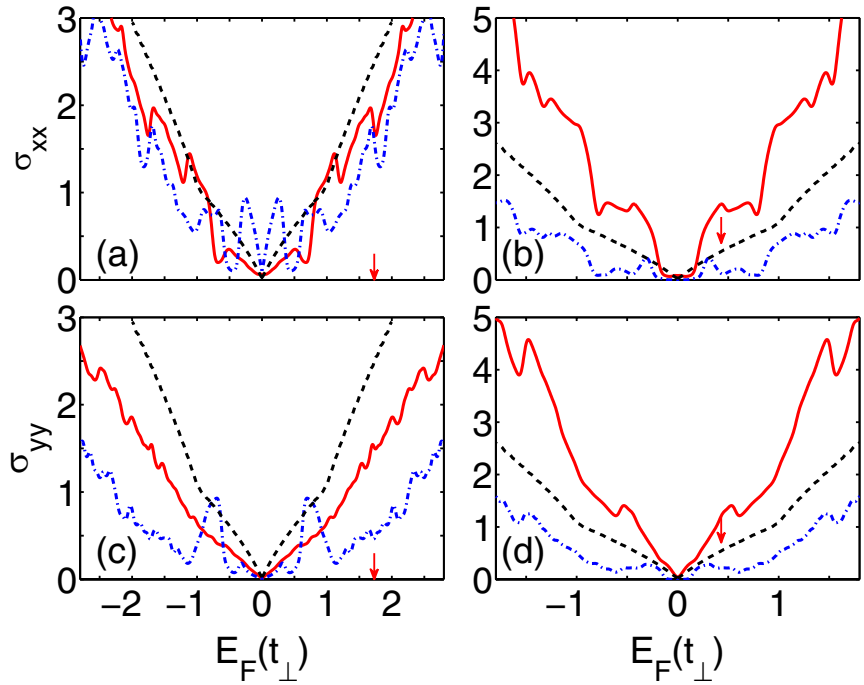

Figure 7. Conductivities σ_{xx} ((a) and (b)) and σ_{yy} ((c) and (d)) against the Fermi energy E_F for the same structures with the DOS presented in figure 6: $L = 3$ ((a) and (c)) and $L = 8$ ((b) and (d)). In each box the curves present the conductivity σ_{xx} (or σ_{yy}) for BLGSLs with $P = 0.1\pi$ (red solid line) or $P = 0.4\pi$ (blue dash–dotted line), and for the pristine BLG (dashed line). Arrows indicate the energy $E_1^{(1,2)}$.

the left box for $L = 3$ the DOS-curve for $P = 0.1\pi$ (red solid) although very close to that of the pristine BLG exhibits a clear dip at the energy $E = E_1^{(1,2)}$. An increase of P makes the DOS-curve more fluctuated, keeping a pair of DPs at $E = 0$ (see the blue dash–dotted curve for $P = 0.4\pi$). In the right box for $L = 8$, the DOS-curve for $P = 0.1\pi$ (red solid) still demonstrates the existence of the zero-energy DPs, while that for $P = 0.4\pi$ (blue dash–dotted) clearly shows a direct band gap (of $\approx 0.3t_\perp$ in width) and a deep local minimum at $E = E_1^{(1,2)}$.

An accurate reflection of the DOS discussed in figure 6 could be found in the conductivity. Figure 7 shows the conductivities σ_{xx} ((a) and (b)) and σ_{yy} ((c) and (d)) plotted versus the Fermi energy E_F for the same BLGSLs as those analysed in figure 6, including the conductivities of the pristine BLG (the dashed curves, they are identical in all boxes). The common features of the conductivities of all the BLGSLs studied in figure 7 are (i) the conductivities are symmetrical with respect to the sign of the Fermi energy. (Such a conductivity symmetry is a direct consequence of

the symmetry of the DOS with respect to the sign of the energy.) and (ii) both σ_{xx} and σ_{yy} strongly fluctuate against E_F and, additionally, for a given L the fluctuation in σ_{xx} is stronger than that in σ_{yy}. (Such a conductivity fluctuation results from the fluctuation in the DOS: the conductivity goes up (down) as the Fermi energy moves through a peak (dip) in the DOS).

Comparing the boxes in figure 7 reveals some additional features, as follows: (i) For BLGSLs with $L = 3 < L_C$ ((a) and (c)) both the conductivities σ_{xx} and σ_{yy} are on average smaller than the conductivity of the pristine BLG and decrease slightly with increasing P; (ii) For BLGSLs with $L = 8 > L_C$ ((b) and (d)) the conductivities are much more (unsystematically) sensitive to a change in P, showing the existence of a direct band gap in the case of $P = 0.4\pi$; and (iii). For the BLGSLs with $L = 3$ the conductivity σ_{xx} shows an impressive dip at the Fermi energy corresponding to the lowest finite-energy TP $E_1^{(1,2)}$ (indicated by the arrow), while for the BLGSLs with $L = 8$ the effect of this TP in the conductivities is weaker in the case of $P = 0.4\pi$ and almost invisible in the case of small P (red solid curve for $P = 0.1\pi$ in (b)).

We recall that apart from the finite-energy TPs identified at zero wave-number, there are also the finite-energy TPs located at $k_x \neq 0$ which should certainly affect the DOS and the conductivity behaviours.

5. Conclusions

We have studied the energy band structure of the BLGSLs with zero-averaged periodic δ-function potentials (arranged along the x-direction) within the framework of the four-band continuum model, using the transfer matrix method. Our analysis has been focused on the TPs between adjacent minibands which produce a certain effect on the transport properties. For the zero-energy TPs at $k_y = 0$ claimed previously, we were able to show the Dirac-like dispersion relation, which may be either isotropic or strongly anisotropic, depending on the potential strength. We also show that the direct band gap can be opened only in the energy spectrum of the BLGSLs with large enough potential periods ($L > L_C$).

From the finite-energy TPs we are able to identify exactly those located at zero wave-number. It was shown that in the vicinity of the finite-energy TPs identified, the dispersion is direction-dependent in the sense that it is linear or parabolic in the k_x- or k_y-direction, respectively. Additionally, numerical calculations show that the 'electron'- and the 'hole'-mass in the parabolic dispersion in the k_y-direction may be different in both value and sign, depending on the periodic potential parameters. The TPs at zero- as well as finite-energies may find themselves reflected in the oscillating behaviour of the density of states and the conductivities which have been calculated for BLGSLs of different potential parameters.

Acknowledgments

This work was financially supported by The Vietnam National Foundation for Science and Technology Development under Grant No. 103.02-2013.17. We thank Ms N T Thuong for helpful discussions.

Appendix

We describe how the central equation (3) can be derived. Following the general idea of the T-matrix method [22], we first consider the wave functions of the equation $H\Psi = E\Psi$ in the regions of constant potential, $V(x) = V_0 = \text{constant}$. For H of equation (1) these functions can be generally written in the form $\Psi = QR(x)[A, B, C, D]^T \exp(ik_y y)$. They can be then simplified by the linear transformation $Q \to \mathcal{T}Q$ with [15]

$$\mathcal{T} = \frac{1}{2}\begin{pmatrix} 1 & 0 & -1 & 0 \\ 0 & 1 & 0 & -1 \\ 1 & 0 & 1 & 0 \\ 0 & 1 & 0 & 1 \end{pmatrix}. \tag{A.1}$$

So

$$Q \to \mathcal{T}Q = \begin{pmatrix} 1 & 1 & 0 & 0 \\ k_1/E' & -k_1/E' & -ik_y/E' & -ik_y/E' \\ 0 & 0 & 1 & 1 \\ -ik_y/E' & -ik_y/E' & k_2/E' & -k_2/E' \end{pmatrix}, \tag{A.2}$$

while the $\mathcal{T}$-transformation does not change the matrix $R(x)$:

$$R(x) = \text{diag}\left[e^{ik_1 x}, e^{-ik_1 x}, e^{ik_2 x}, e^{-ik_2 x}\right], \tag{A.3}$$

where $E' = E - V_0$ and $k_n = \sqrt{E'^2 - (-1)^n E' - k_y^2}$ with $n = 1, 2$.

Furthermore, the amplitudes $\mathcal{A}_I$ of the wave function before a unit cell and those after it, $\mathcal{A}_F$, could be related to each other by the T-matrix

$$\mathcal{A}_F = T(F, I)\mathcal{A}_I. \tag{A.4}$$

On the other hand, Bloch's theorem states

$$Q_I R_I(x)\mathcal{A}_F = \exp(ik_x L) Q_I R_I(x - L)\mathcal{A}_I, \tag{A.5}$$

where k_x is the Bloch wave number and L is the period of $V(x)$.

Comparing equations (A.4) and (A.5) gives rise to equation (3),

$$\det\left[T - e^{ik_x L} R_I^{-1}(L)\right] = 0. \tag{A.6}$$

For the δ-function potential $V(x)$ of equation (2) the unit cell is described in figure 1(a) and the $T(F, I)$-matrix in equation (A.6) is defined as

$$T(F, I) = [R_I(L/2)]^{-1} Q_I^{-1} S(-P) S' S(P) Q_I,$$

where Q_I and R_I are defined respectively in equations (A.2) and (A.3) for $V_0 = 0$, $S' = Q_I R_I(L/2) Q_I^{-1}$, and

$$S(P) = \begin{pmatrix} \cos(P) & -i\sin(P) & 0 & 0 \\ -i\sin(P) & \cos(P) & 0 & 0 \\ 0 & 0 & \cos(P) & -i\sin(P) \\ 0 & 0 & -i\sin(P) & \cos(P) \end{pmatrix}.$$

References

[1] Castro Neto A H, Guinea F, Peres N M R, Novoselov K S and Geim A K 2009 *Rev. Mod. Phys.* **81** 109

[2] Das Sarma S, Adam S, Hwang E H and Rossi E 2011 *Rev. Mod. Phys.* **83** 407

[3] Castro E V, Novoselov K S, Morozov S V, Peres N M R, Lopes dos Santos J M B, Nilsson J, Guinea F, Geim A K and Castro Neto A H 2010 *J. Phys.: Condens. Matter* **22** 175503

[4] McCann E and Koshino M 2013 *Rep. Prog. Phys.* **76** 056503

[5] Geim A K and Grigorieva I V 2013 *Nature* **499** 419

[6] Park C-H, Yang L, Son Y-W, Cohen M L and Louie S G 2008 *Nat. Phys.* **4** 213
Park C-H, Yang L, Son Y-W, Cohen M L and Louie S G 2008 *Phys. Rev. Lett.* **101** 126804
Park C-H, Yang L, Son Y-W, Cohen M L and Louie S G 2009 *Phys. Rev. Lett.* **103** 046808

[7] Brey L and Fertig H A 2009 *Phys. Rev. Lett.* **103** 046809

[8] Barbier M, Vasilopoulos P and Peeters F M 2010 *Phys. Rev.* B **81** 075438

[9] Pham C H, Nguyen H C and Nguyen V L 2010 *J. Phys.: Condens. Matter* **22** 425501

[10] Ghosh S and Sharma M 2009 *J. Phys.: Condens. Matter* **21** 292204

[11] Masir M R, Vasilopoulos P and Peeters F M 2010 *J. Phys.: Condens. Matter* **22** 465302

[12] Snyman I 2009 *Phys. Rev.* B **80** 054303

[13] Dell' Anna L and De Martino A 2011 *Phys. Rev.* B **83** 155449

[14] Le V Q, Pham C H and Nguyen V L 2012 *J. Phys.: Condens. Matter* **24** 345502

[15] Barbier M, Vasilopoulos P and Peeters F M 2010 *Phys. Rev.* B **82** 235408

[16] Killi M, Wu S and Paramekanti A 2011 *Phys. Rev. Lett.* **107** 086801

[17] Tan L Z, Park C-H and Louie S G 2011 *Nano Lett.* **11** 2596

[18] Kusminskiy S V, Campbell D K and Castro Neto A H 2009 *Eur. Phys. Lett.* **85** 58005

[19] Henriksen E A, Jiang Z, Tung L-C, Schwartz M E, Takita M, Wang Y-J, Kim P and Stormer H L 2008 *Phys. Rev. Lett.* **100** 087403

[20] Henriksen E A and Eisenstein J P 2010 *Phys. Rev.* B **82** 041412

[21] Zou K, Hong X and Zhu J 2011 *Phys. Rev.* B **84** 085408

[22] Nguyen H C and Nguyen V L 2009 *J. Phys.: Condens. Matter* **21** 045305

[23] Malko D, Neiss C, Viñes F and Görling A 2012 *Phys. Rev. Lett.* **108** 086804

[24] Soodchomshom B, Tang I-M and Hoonsawat R 2013 *J. Appl. Phys.* **113** 073710